Title: Light Activated BioID (LAB): an optically activated proximity labeling system to study protein-protein interactions.

Authors: Omer Shafraz [‡], Carolyn Marie Orduno Davis [‡], Sanjeevi Sivasankar [*].

Affiliation: Department of Biomedical Engineering, University of California, Davis, 95616, CA.

[‡] Contributed equally to this work.

* To whom correspondence should be addressed. Email: ssivasankar@ucdavis.edu.

Abstract

Proximity labeling with genetically encoded enzymes is widely used to study protein-protein interactions in cells. However, the resolution and accuracy of proximity labeling methods are limited by a lack of control over the enzymatic labeling process. Here, we present a high spatial and temporal resolution technology that can be activated on demand using light, for high accuracy proximity labeling. Our system, called Light Activated BioID (LAB), is generated by fusing the two halves of the split-TurboID proximity labeling enzyme to the photodimeric proteins CRY2 and CIB1. Using live cell imaging, immunofluorescence, western blotting, and mass spectrometry, we show that upon exposure to blue light, CRY2 and CIB1 dimerize, reconstitute the split-TurboID enzyme, and biotinylate proximate proteins. Turning off the light halts the biotinylation reaction. We validate LAB in different cell types and demonstrate that it can identify known binding partners of proteins while reducing background labeling and false positives.

47 **Introduction:**

48 Protein-protein interactions (PPIs) are essential for cellular function, and decoding these
49 interactions are crucial for understanding biological pathways in health and disease. While many
50 methods have been developed to map protein interactomes (Qin et al., 2021), proximity labeling
51 (PL) techniques are among the most widely used approaches, since they capture transient,
52 dynamic PPIs in the near-native cellular environment.

53 PL employs enzymes such as promiscuous biotin ligases for proximity-dependent biotin
54 identification (BioID) (Choi-Rhee et al., 2004; Kim et al., 2016; Ramanathan et al., 2018; Roux et
55 al., 2012), peroxidases for peroxide-dependent biotin identification (APEX) (Martell et al., 2012),
56 horseradish peroxidase (HRP) (Kotani et al., 2008), or Pup ligase PafA in PUP-IT (Liu et al., 2018).
57 These enzymes are genetically fused to a protein of interest (the *bait*) and generate short-lived
58 intermediate reactive biotins that covalently tag neighboring proteins (the *prey*). Other methods
59 of tagging include using photosensitizers such as the enzyme miniSOG (Zhai et al., 2022) or
60 photocatalyst-antibody conjugates to generate singlet oxygen (Müller et al., 2021) or activated
61 carbenes (Geri et al., 2020) as alternate intermediates for targeting biotin-tagged probes.
62 Subsequently, biotin-tagged prey proteins are enriched using streptavidin-coated beads and
63 identified using mass spectrometry (MS).

64 BioID is preferred over other PL methods in many *in vitro* and *in vivo* applications, since
65 peroxidases such as APEX and HRP require the addition of hydrogen peroxide and miniSOG
66 produces reactive oxygen species, which can both be toxic to cells. However, BioID has long
67 labeling times (>18 hrs) and requires an optimal temperature of 37° C (Roux et al., 2012). In an
68 effort to improve BioID's performance, TurboID has been introduced as a fast-labeling biotin ligase
69 (10 min labeling time) that also retains activity at temperatures <37° C, which enables it to be

70 used in organisms like flies, worms, yeast (Branon et al., 2018), and plants (Mair et al., 2019), as
71 well as in cell culture (Shafraz et al., 2020). However, TurboID can biotinylate proteins using
72 endogenous cellular biotin, which creates a large labeling background as well as cellular toxicity.
73 To overcome this limitation, a 'split-TurboID' technology was recently introduced, which splits the
74 TurboID enzyme into two inactive halves that only induce biotinylation when reconstituted by the
75 addition of a chemical cofactor, rapamycin. While this reduces background labeling and increases
76 spatial specificity (Cho et al., 2020a), the requirement that both halves of Split-TurboID be
77 expressed in close proximity creates a level of background biotinylation unrelated to the addition
78 of the cofactor (Cho et al., 2020b). Additionally, usage of a cofactor introduces the possibility of
79 uncontrolled effects on cellular processes, and the time resolution is limited by the cofactor's
80 ability to diffuse to the cell compartment of interest. Furthermore, the difficulty of removing the
81 factors from the media makes it difficult to control the cessation of the biotinylation reaction
82 (Klewer and Wu, 2019).

83 These limitations in conventional proximity labeling can be overcome by developing new
84 classes of proximity labeling technologies that can be activated on demand without the addition
85 of chemical cofactors, and with high spatial and temporal control. We therefore designed a
86 proximity labeling technology that is precisely triggered using blue (488 nm) light. Our system,
87 called Light Activated BioID (LAB), is generated by fusing the two halves of the split-TurboID
88 enzyme to genetically encoded *Arabidopsis thaliana* photodimeric proteins cryptochrome 2
89 (CRY2) and cryptochrome-interacting basic-helix-loop-helix (CIB1) (Liu et al., 2008). Upon
90 exposure to blue light, CRY2 and CIB1 dimerize within 300 ms (Kennedy et al., 2010; Taslimi et
91 al., 2016) and reconstitute the two halves of the split-TurboID enzyme, thereby inducing
92 biotinylation. Since the photodimers have a half-life of ~6 minutes (Kennedy et al., 2010; Taslimi
93 et al., 2016), dissociation of CRY2 and CIB1 re-splits the TurboID and halts biotinylation. Since

94 LAB dissociates within minutes after the blue light is turned off, background biotinylation is
95 reduced and false positives as well as cellular toxicity due to over-biotinylation are minimized.

96 Here, as a proof of concept, we use live cell imaging, immunofluorescence, western blots,
97 and mass spectrometry (MS) to show in Human Embryonic Kidney (HEK) 293T cells that LAB
98 dimerizes and biotinylates proximal proteins when exposed to blue light. Next, by fusing LAB to
99 the ubiquitous cell-cell adhesion protein E-cadherin (Ecad) in Madin-Darby canine kidney (MDCK)
100 cells, we demonstrate that LAB can map Ecad's known binding partners in a light-dependent
101 manner, with higher accuracy and significantly fewer false positives compared to stand-alone
102 TurboID.

103

104 **Results:**

105 **LAB dimerizes upon blue light illumination:** We developed genetically encodable LAB
106 constructs by fusing previously reported low-affinity split-TurboID (L73/G74) (Cho et al., 2020a)
107 onto light-inducible dimerizing plant proteins CRY2 and CIB1. The N-terminal fragment of split-
108 TurboID (spTN) and CIB1 were fused onto plasma membrane-targeted enhanced Green
109 Fluorescent Protein (pmEGFP). The C-terminal split TurboID fragment (spTC) and CRY2 were
110 fused onto mCherry and expressed in the cytoplasm (Fig. 1a). We hypothesized that, upon blue
111 light exposure, CRY2-spTC-mCherry (*henceforth referred to as CryC*) would translocate to the
112 plasma membrane and bind to CIB1-spTN-pmEGFP (*henceforth referred to as CibN*) (Fig. 1a).

113 We transiently expressed both constructs in HEK293T cells and observed that CryC was
114 distributed throughout the cytoplasm while CibN was localized at the plasma membrane (Fig. 1b).
115 When illuminated with a 488 nm laser, CryC translocated to the plasma membrane within seconds

116 of laser exposure; the residual mCherry signal in the cytoplasm even after laser exposure arose
117 because CryC was expressed at high enough levels to saturate CibN on the membrane (Fig. 1b).
118 When the laser beam was turned off, CryC dissociated back to the cytoplasm in ~10 mins (Fig.
119 1b). These kinetics show that the fused constructs don't alter the previously reported CRY2/CIB1
120 kinetics (Kennedy et al., 2010). Furthermore, when a selected region of the plasma membrane
121 was illuminated with a 488 nm laser, CryC began accumulating in under a second and reached
122 maximum accumulation in seconds (Fig. 1 c, d, e). This demonstrates that LAB can be activated
123 in selected regions of the cell and split-TurboID will be bound for ~ 10 mins from the end of
124 illumination, biotinylating neighboring proteins and giving more temporal and spatial control over
125 previous PL systems.

126

127 **LAB biotinylates only in the presence of blue light and biotin:** Since split-TurboID
128 shows significant biotin labeling after 1hr (Cho et al., 2020a), we transiently co-expressed CibN
129 and CryC in HEK cells and exposed the cells to alternating 10-minute cycles of blue light (470
130 nm) and darkness for 1hr using a blue LED light in the presence of 100 μM biotin (Fig. 2a). We
131 then fixed the cells and stained them for GFP, mCherry, and biotin using anti-GFP and anti-
132 mCherry antibodies and Alexa-647 conjugated streptavidin (Sta) (Fig. 2 b-g, S1-6). Next, we
133 measured the level of CibN, CryC, and Sta on the membrane; fluorescence intensities were
134 normalized to CibN fluorescence intensity to account for differences in CibN expression levels in
135 different cells (Fig. 2h, table S1). We also quantified the colocalization of CryC and Sta with
136 membrane bound CibN (Fig. 2i, table S2). All p-values are catalogued in the supplementary
137 information (tables S3, S4).

138 In the presence of light and biotin, CryC showed a high colocalization with CibN at the
139 plasma membrane, which resulted in high Sta fluorescent intensity corresponding to significant
140 membrane proximal biotinylation (Figs. 2 b, h, i, S1, table S1, table S2). When samples were kept
141 in darkness, the CryC did not localize to the membrane and no biotinylation was observed (Fig. 2
142 c, h, i, S2, table S1, table S2). Similarly, when cells were exposed to light in the absence of biotin,
143 CryC had significant membrane fluorescence intensity and colocalization with CibN (Fig. 2 d, h, i,
144 S3, table S2), but did not result in significant biotinylation, since Sta fluorescent intensity was very
145 low at the membrane with negligible colocalization between Sta and CibN (Fig. 2 h, i, table S2).
146 Furthermore, in the absence of both light and biotin, very low membrane CryC and Sta
147 fluorescence intensity and CibN colocalization were measured corresponding to negligible
148 biotinylation (Fig. 2 e, h, i, S4, table S1, table S2). Finally, no biotinylation was measured when
149 only CryC (Fig. 2f, S5) or CibN (Fig. 2g, S6) was expressed. Hence, the immunofluorescence
150 data demonstrate that CibN and CryC dimerize and biotinylate only when exposed to blue light.

151

152 **Ecad-LAB activity is light-dependent:** Next, to validate LAB activity with a well-
153 characterized protein and in a different cell line, we fused LAB to the ubiquitous, transmembrane
154 protein E-cadherin (Ecad) in MDCK cells. Ecad is an essential cell-cell adhesion protein that plays
155 key roles in the formation and maintenance of epithelial tissues and acts as a tumor suppressor
156 (Xie et al., 2022). Besides binding homophilically, Ecad also has many recorded heterophilic
157 transmembrane binding partners such as the desmosomal adhesion proteins Desmoglein-2
158 (Dsg2) and Desmocollin-3 (Dsc3) (Shafraz et al., 2020). We fused CIB1 and spTN onto Ecad-
159 EGFP (ECibN) (Fig. 3a) and stabily expressed it with CryC in MDCK cells containing endogenous
160 Ecad.

161 First, we confirmed that Ecad-CibN localizes to cell-cell junctions (Fig. 3b, S7-S12). Next,
162 cells were exposed to alternating 10 min cycles of blue light and darkness for 1hr before fixing
163 and immunostaining and CryC accumulation at the junction was monitored. To measure
164 biotinylation and localization, ECibN, CryC, and Sta fluorescence intensity (normalized by ECibN
165 fluorescence intensity to account for variation in ECibN expression levels) were measured. The
166 high CryC and Sta fluorescence intensity near the membrane in the presence of light and biotin
167 confirmed biotinylation activity, with high colocalization coefficients for ECibN with both CryC and
168 Sta (Fig. 3 b, h, i, S7, table S5, S6). In the absence of light and the presence of exogenous biotin,
169 CryC did not colocalize with ECibN, and a low membrane intensity and colocalization coefficient
170 was measured (Fig. 3 c, h, i, S8, table S6). Additionally, no biotinylation was detected, with a
171 negligible Sta membrane intensity and colocalization coefficient between ECibN and Sta (Fig. 3
172 c, h, i, S8, table S5, S6). This indicates that Ecad-LAB biotinylation is light dependent.
173 Furthermore, when cells were illuminated with blue light in the absence of biotin, even though
174 ECibN and CryC showed colocalization and CryC had an increased membrane intensity (Fig. 3
175 d, h, i, S9, table S6), the relative Sta intensity and colocalization was not significant (Fig. 3 d, h, i,
176 table S5, S6). Similarly, in the absence of both light and biotin, ECibN/CryC did not colocalize or
177 show a substantial CryC or Sta membrane signal, with no colocalization between ECibN and Sta
178 (Fig. 3 e, h, i, S10, table S6). Finally, when only CryC (Fig. 3f, S11) or ECibN (Fig. 3g, S12) was
179 expressed, there was no biotinylation observed. Thus, the immunofluorescence data for ECibN
180 and CryC in MDCK cells confirm that LAB can be applied to other proteins of interest, in different
181 cell lines, and that when exogenous biotin is provided, its biotinylation activity depends only on
182 exposure to light. All p-values are catalogued in supplementary information (tables S7, S8). It is
183 important to note that the presence of a high background in the Sta channel for MDCK cells was
184 due to a low ECibN expression level and not due to off-target biotinylation since the background
185 levels for the biotin positive and negative conditions were similar (Fig. 3 b-e).

186 Finally, to quantify how quickly Ecad-LAB biotinylates proximal proteins, we performed
187 immunofluorescence analysis for MDCK cells exposed to light for different durations (1min,
188 10min, and 30min; Fig. S13). The data shows statistically significant biotinylation after just 1min
189 of light exposure, indicating that Ecad-LAB is indeed biotinylating on this timescale (Fig. S13 a,
190 d, e).

191

192 **Benchmarking LAB against stand-alone TurboID:** To benchmark LAB performance, we
193 compared Ecad proteomes generated using both LAB and stand-alone full-length TurboID. A
194 biotinylated LAB proteome was generated using MDCK cells stably expressing Ecad-LAB. The
195 cells were incubated in 100μM biotin and were either exposed to blue light for 1 hr using 10 min
196 on/off cycles or were kept in darkness. To generate a corresponding biotinylated TurboID
197 proteome, MDCK cells were stably transfected with Ecad conjugated to full-length TurboID (Ecad-
198 Turbo). The Ecad-Turbo cells were either incubated with or without 100μM biotin for 1hr. The
199 biotinylated proteins generated by Ecad-LAB and Ecad-Turbo were then captured from the
200 corresponding cell lysate using streptavidin-coated magnetic beads. The captured proteins were
201 trypsin digested before LC-MS/MS was performed for three replicates per condition (Ecad-LAB)
202 or two replicates per condition (Ecad-Turbo).

203 The Ecad-LAB MS data showed significant enrichment of proteins in cells illuminated with
204 blue light compared to those kept in darkness (Fig. 4a). We then compared Ecad-LAB hits in the
205 presence and absence of light against Ecad-Turbo in the presence and absence of biotin (Fig. 4).
206 This data demonstrated that Ecad-LAB had 300 positive hits and only 3 negative hits (Fig. 4a). In
207 contrast, Ecad-Turbo had 247 positive hits and 139 negative hits (Fig. 4b). Well-established
208 members of the core Ecad/catenin complex (Guo et al., 2014) such as Ecad, β-catenin, α-catenin,

209 p120-catenin, and vinculin were highly enriched in Ecad-LAB. Similarly, well-established Ecad
210 transmembrane binding partners such as Dsg2 and Dsc3 were prominent hits in Ecad-LAB
211 (Shafraz et al., 2020) (Fig. 4a). Importantly, all the hits (positive candidates, negative candidates,
212 and non-candidates) in Ecad-LAB were also hits in Ecad-Turbo, with the expected exceptions of
213 the light-activated dimer components (Cry/CIB) (Fig. 4c). This demonstrates that Ecad-LAB is at
214 least as accurate as Ecad-Turbo, with an increased precision resulting in fewer extraneous hits.

215 Comparison of the ratio of positive/negative signal levels for Ecad and its key binding
216 partners (highlighted in Fig. 4a) demonstrated that Ecad-LAB has a universally higher
217 signal/background ratio compared to Ecad-Turbo (Fig. 4d). This trend extended for the entire
218 Ecad-LAB interactome as seen in the signal/background ratios for broad categories of proteins
219 (Fig. 4e). In this figure the Ecad-LAB interactome was sorted into previously published categories
220 (Shafraz et al., 2020) as described in the figure legend. We further directly compared the biotin
221 negative and light negative conditions of Ecad-Turbo and Ecad-LAB respectively, which showed
222 an almost universally higher absolute protein level present in the negative Ecad-Turbo condition
223 compared to the negative Ecad-LAB condition (Fig. S14). Taken together, this data quantitatively
224 demonstrates that LAB has a significantly lower background biotinylation than conventional
225 TurboID.

226 We also used MS to confirm LAB's activity in HEK293T cells transiently co-expressing
227 CibN and CryC. As described above for Ecad-LAB, the cells in the presence of biotin were either
228 exposed to blue light or darkness and biotinylated proteins were isolated, trypsin digested and
229 analyzed using LC-MS/MS (three replicates per condition). MS data showed significant
230 enrichment of proteins in cells illuminated with blue light compared to those kept in darkness (Fig.
231 S15a). Although membrane-bound GFP does not have any prey in HEK293T cells, CIB1 and GFP,
232 which are close to the Split-TurboID, served as proxy prey and were significantly enriched (Fig.

233 S15a). Finally, principal component analysis (PCA) showed two separate clusters for the light-
234 exposed samples and the controls, implying distinctive variations between both groups (Fig.
235 S15b).

236

237 **Benchmarking biotinylation efficiency of LAB against stand-alone TurboID:** We used
238 western blots to benchmark the biotinylation efficiency of Ecad-LAB exposed to light for different
239 durations (1hr, 3hrs, 5hrs, 18hrs) against Ecad-Turbo incubated in biotin for 10 mins (Fig. S16).
240 To prevent phototoxicity in Ecad-LAB cells due to their long exposure to blue-light, a shorter on/off
241 light cycle (1min on : 5min off) was used. Western blots were performed on whole cell lysates with
242 an equal amount of protein loaded in each lane; biotinylated proteins were stained with anti-biotin
243 HRP.

244 While Ecad-Turbo incubated with biotin for 10 mins had higher biotinylation levels than
245 Ecad-LAB at all measured timepoints (Fig. S16a), the larger number of false positives in Ecad-
246 Turbo (Figs. 4, S14) made a direct comparison of biotinylation from western blot bands difficult.
247 We therefore compared the biotinylation efficiency of Ecad-LAB for 1 time point (1 hr) against
248 Ecad-Turbo and used a single band at ~130kDa, which is present in the Ecad-LAB and Ecad-
249 Turbo lanes (but not in the untransfected control), for subsequent analysis (Fig. S16a, S16b).

250 It is important to note that while every Ecad-Turbo protein is capable of biotinylating a
251 target, Ecad-LAB has a Pearson's correlation coefficient of 0.44 (see Fig. 3), implying that only
252 ~44% of ECibN proteins are bound to CryC and capable of biotinylating. Furthermore, differences
253 in the expression levels of ECibN and Ecad-Turbo could also impact biotinylation efficiency. We
254 therefore intensity corrected the Ecad-Turbo and Ecad-LAB lanes for their differing expression
255 levels (determined using an Ecad western blot, Fig. S16c) and for ECibN/CryC colocalization

256 (using experimentally determined Pearson's coefficients, Fig. 3). The intensity corrected bands
257 were used to directly compare the relative efficiencies of Ecad-Turbo and Ecad-LAB (Fig. S16 d-
258 f). The ratio between the positive and negative condition bands for each construct showed that
259 intensity corrected Ecad-LAB with 1 hour light exposure had a similar biotinylation efficiency as
260 Ecad-Turbo incubated with biotin for 10 minutes (Fig. S16f). In contrast, stand-alone Split-TurboID
261 (albeit in non-correlation corrected data) needed 4 hours to approach 1 minute of full-length
262 TurboID labeling (Cho et al., 2020b).

263 To compare biotinylation efficiency of LAB and stand-alone TurboID in HEK cells, we
264 transiently expressed a full TurboID construct (CIB1-TurboID-pmEGFP) and incubated in 100 μM
265 biotin for 1 hr. We also transiently co-expressed CryC with CibN in HEK cells and exposed these
266 cells to blue light in the presence of biotin for 10 min on/off intervals for 1 hr. Both cells were then
267 lysed and biotinylated proteins were captured using streptavidin-conjugated beads and used for
268 western blots, with the eluted protein stained with Sta-HRP (Fig. S17). Western blots showed
269 significantly higher biotinylation in light-exposed HEK293T cells compared to cells kept in
270 darkness. However, the biotinylation efficiency of LAB was less than cells expressing TurboID,
271 likely due to the lower activity and background from LAB (Fig. S17a).

272 While we did not have any known prey for CibN in HEK293T cells, we expected the GFP
273 and mCherry portions of CibN and CryC to be biotinylated, as these would be directly proximal to
274 the reconstituted Split-TurboID. When we stained eluted protein with GFP and mCherry
275 antibodies, we found a much higher presence of these proteins in the light-positive condition than
276 the light negative condition, with no staining occurring on a blank control (Fig. S17 b, c). This
277 confirms that LAB biotinylates proximal proteins in a light-dependent manner and identifies
278 expected binding partners.

279

280 **Discussion:**

281 For LAB, we used split-TurboID as the labeling enzyme due to its well characterized
282 biotinylation kinetics. Similarly, we used the photodimer pair CRY2 and CIB1 because they are
283 one of the most widely-used photodimer systems, and have been tested in many different cell
284 lines as well as in living organisms to investigate a wide variety of cellular functions (Taslimi et al.,
285 2016). Importantly, CRY2/CIB1 binding kinetics complement those of Split-TurboID by remaining
286 associated long enough after light exposure to allow for sufficient biotinylation, while not remaining
287 bound too long post-exposure so that the labeling reaction can be arrested with the removal of
288 light.

289 Using immunofluorescence, western blots, and MS, in both HEK293T and MDCK cells,
290 we demonstrated that LAB can be selectively activated through researcher-controlled biotin and
291 light application. We were able to demonstrate statistically significant biotinylation after only one
292 minute of light exposure, showing that functional complementation of LAB is achieved on a rapid
293 timescale (Fig. S13a). LAB's specificity was validated through MS analysis showing light
294 exposure-dependent enrichment of many proteins known to bind to Ecad, including the α/β-
295 catenin/vinculin complex that links Ecad to the actin cytoskeleton (Fig. 4a). Importantly, these and
296 other known Ecad binding partners were highly enriched in the light positive condition compared
297 to the light negative condition, with a signal to background ratio an order of magnitude higher than
298 that of Ecad-conjugated full-length TurboID under biotin positive and negative conditions (Fig. 4e).
299 Additionally, not every major Ecad binding partner was successfully detected as a positive
300 candidate by Ecad-Turbo, possibly a result of its high background labeling reducing data

301 resolution (Fig. 4b). Taken together, this shows that LAB successfully labels proximal proteins in
302 a light-dependent manner with higher specificity than full-length TurboID.

303 Since LAB uses split-TurboID and light for biotinylation, it is reasonable to expect that LAB
304 will efficiently biotinylate target proteins in different cellular compartments. It has already been
305 demonstrated that both split-TurboID (Cho et al., 2020b) and stand-alone TurboID (Branon et al.,
306 2018) are capable of biotinylating target proteins in different organelles with distinct pH, redox
307 environments, and endogenous nucleophile concentrations. Additionally, since LAB relies on light
308 rather than a diffusion-limited chemical cofactor, it can easily be activated in different cellular
309 compartments. The main consideration will be expressing LAB sufficiently in different
310 compartments, which is more a function of construct and bait design than of its biotinylation ability.
311 Importantly, truncated versions of the CRY2 and CIB1 proteins have been developed (Taslimi et
312 al., 2016), that can be used in LAB if large constructs would affect expression and localization of
313 bait proteins tagged with LAB.

314 It has previously been shown that CRY2 can homodimerize when illuminated with blue
315 light (Wang and Lin, 2020). However, this is not an issue for LAB since our construct only has the
316 inactive C-terminus of Split-TurboID associated with CRY2. Consequently, CRY2
317 homodimerization cannot reconstitute a functional TurboID. This is supported by our data showing
318 that no biotinylation is observed in the CryC-only condition (Fig. 2f). Furthermore, previous studies
319 show that CRY2 homodimerization does not prevent interaction with CIB1 (Bugaj et al., 2013).

320 A consideration when using LAB is the possibility of phototoxicity after long-duration
321 exposure to the activating blue light source. Due to Cry/CIB's binding half-life of approximately 5
322 minutes, alternating 10- minute cycles of light and darkness allowed significant dimerization and
323 biotinylation, while reducing phototoxicity for our shorter-term (< 1 hr) experiments. For longer

duration experiments (see Fig. S16), we used a shorter light cycle (1min on, 5min off) to further reduce phototoxic effects while still maintaining maximal Ecad-LAB activation. However, for even longer-term experiments, the optimal light intensity and exposure cycle will likely need to be determined based on the cells and application.

Recently, a different opto-dimerization system, iLID, has been used with a new split-TurboID variant (Chen et al., 2022). However, iLID has a half-life of under a minute (Kennedy et al., 2010; Taslimi et al., 2016), which may not provide enough time for appreciable labeling to occur before the dimers unbind and inactivate Split-TurboID. Furthermore, in this opto-dimerization study, TurboID was split at a previously uncharacterized location (G99/E100) and consequently, the rate of biotinylation of this new split-TurboID variant is unknown (Chen et al., 2022).

Another PL tool using light-activated miniSOG has been recently developed (PDPL), which uses singlet oxygen to create electrophilic residues on prey proteins, which can be subsequently bound to an alkyne chemical probe and pulled down using click chemistry (Zhai et al., 2022). However, the aniline probe used with PDPL can be toxic to cells (Wang et al., 2016; Zhai et al., 2022). Furthermore, miniSOG has a labeling radius of up to 70nm, which is much larger than TurboID's 10nm labeling radius (Kim et al., 2014). While a larger labeling radius is appropriate for identifying compartmentalization of proteins, LAB's smaller labeling radius is more suited for discovering direct PPIs (Cho et al., 2020b; Zhai et al., 2022). Another light-activated PL tool, MicroMap, which uses an antibody conjugated to an iridium photocatalyst to label nearby proteins via carbene intermediates, has also recently been developed (Geri et al., 2020; Seath et al., 2021). However, the necessity of a primary antibody that binds to the bait protein at a convenient location limits MicroMap's applications.

347 Unlike CRY2 and CIB1 which photodimerize in the presence of blue light,
348 photodimerization activated by longer wavelength light could be more effective for PPI
349 identification in deeper tissue. However, the two known red light activated photo-hetrodimers
350 (PhyB/PIF3 and PhyB/PIF6), require light exposure at different wavelengths for both activation
351 and inactivation (Klewer and Wu, 2019). We therefore chose a photodimer pair that dissociated
352 in the dark, rather than through alternate wavelength exposure, for ease of use. Importantly, since
353 CRY2/CIB1 dimerization can be triggered using two-photon excitation (Kennedy et al., 2010), this
354 may allow LAB to map PPIs in deeper tissue *in vivo*.

355 We anticipate that the ability to activate LAB using light, coupled with its high temporal
356 resolution, can be exploited to interrogate differences in PPIs at different time points in the cell
357 cycle. We also expect that by using focused activating light, LAB can be used to identify
358 differences in PPIs at distinct cellular locations. Finally, like TurboID, which has previously been
359 used to map extracellular PPIs (Shafraz et al., 2020), we anticipate that LAB can also be used to
360 investigate extracellular protein interactions with high spatial and temporal resolution.

361

362 **Materials and Methods:**

363 **Cloning of plasmid constructs:** CibN was generated by restriction digesting a CIB-
364 pmEGFP plasmid (Addgene plasmid # 28240, (Kennedy et al., 2010)) at AgeI and NheI sites and
365 fusing PCR amplified CIB1 and spTN (Addgene plasmid # 153002, (Cho et al., 2020a)) using
366 Gibson assembly. SpTN was connected to CIB1 and pmEGFP with linkers V5-KGSGSTSGSGTG
367 (Linker 1) and GSGPVAT. CryC was constructed by inserting PCR amplified spTC (Addgene
368 plasmid #153003, (Cho et al., 2020a)) onto restriction-digested Cry2-mCherry (Addgene plasmid

369 # 26871, (Kennedy et al., 2010)) at XmaI sites with linkers ARGKGSGSTSGSG and
370 KGSGDPPVAT.

371 To design ECibN, V5-spTN-CIB-pmEGFP was constructed by restriction digesting CIB1-
372 pmEGFP with NheI and inserting PCR amplified Linker1-spTN-KGSGAT. Then, Ecad-EGFP
373 plasmid was restriction digested at NotI and XhoI sites and EGFP was reintroduced without the
374 stop codon. Next, NotI and HindIII sites of Ecad-EGFP were restriction digested and PCR
375 amplified V5-spTN-CIB was inserted using Gibson assembly. Ecad-EGFP plasmid was a kind gift
376 from Prof. Soichiro Yamada at the University of California, Davis. All enzymes were high efficiency
377 enzymes from New England Biolabs. All primers used are listed in SI (table S9).

378 For development of a dual-expressing stable Ecad-LAB cell line, a Blasticidin (BSD)
379 resistant CryC plasmid was generated by replacing spTN from Addgene plasmid #153002 (Cho
380 et al., 2020a) using BstBI and NheI enzyme digestion and inserting CryC using Gibson assembly.

381

382 **Cell culture and transfection:** HEK293T cells were grown in High Glucose (4.5 g/L)
383 Dulbecco's modified Eagle's medium (DMEM, Gibco) cell culture media with 10% fetal bovine
384 serum (Gibco) and 1% Penicillin-Streptomycin (PSK) (10,000 U/mL, Life Technologies). MDCK
385 cells were cultured in Low Glucose (1 g/L) DMEM (Gibco) cell culture media with 10% fetal bovine
386 serum and 1% PSK.

387 HEK cells were transiently transfected at 80% confluency with CibN and CryC plasmids
388 using polyethylenimine (PEI) (Polysciences, Inc.). Plasmids and PEI were diluted in Opti-MEM
389 (Gibco) at a 1μg:5μg DNA:PEI ratio. After five minutes, both solutions were mixed and incubated
390 for 90 min and then added to the cells. In order to develop the MDCK stable lines, cells were

391 transfected with the ECibN and BSD-CryC plasmids at 30% confluency using lipofectamine 3000
392 (Invitrogen) with the same DNA ratio. After 24 hours the cells were passaged and sparsely seeded
393 onto p150 dishes. After allowing a further 24 hours for cell attachment and construct expression,
394 500 µg/mL G418 and 5 µg/mL BSD were added to the media for antibiotic selection. Colonies
395 were picked after they reached ~2 mm in size and transferred to a 96 well plate. Colonies were
396 fluorescently imaged to detect expression, and top co-expressing colonies were further expanded.
397 Expanded colonies were further imaged and the brightest clone with the most uniform expression
398 was chosen for experiments.

399

400 **Live cell imaging:** HEK cells were imaged >12 h post-transfection using a 561 nm laser
401 to visualize mCherry and a 488 nm laser to image EGFP and to photo-excite CryC. Images were
402 reconstructed using ImageJ. For the intensity profile of CryC accumulation, a 1µm line was drawn
403 across a selected membrane region and the raw pixel intensity across the line was plotted (Fig.
404 1c). Measurements were taken using ImageJ's Plot Profile analysis feature. To plot CryC
405 accumulation over time, a 0.225µm by 0.900µm box was drawn on the cell membrane bracketing
406 the intensity profile line (Fig. 1c). Measurements for each frame were taken using ImageJ's ROI
407 mean intensity measurement capability.

408

409 **Immunofluorescence:** Cells were transferred to low glucose, phenol red-free DMEM
410 (Gibco) with 10% FBS, incubated with 100 µM biotin and exposed to blue light in 10 min intervals
411 for 1 hr using a blue LED light source (Blue box Pro Transilluminator, miniPCR bio). Control cells
412 were kept in dark. Then, cells were immediately fixed using 3% paraformaldehyde and 0.3% Triton
413 X-100 in phosphate-buffered saline (PBS) for 10 min and blocked with 1% bovine serum albumin

414 (BSA) and 0.3% Triton X-100 in PBS for 30 min. Anti-GFP antibody (rabbit polyclonal, Rockland
415 Immunochemicals) (HEK293T cells), Anti-GFP antibody (chicken polyclonal, Rockland
416 Immunochemicals) (MDCK cells), Alexa Fluor 488-conjugated Goat anti-rabbit antibody (Life
417 Technologies) (HEK293T cells), and Alexa Fluor 488-conjugated Goat anti-chicken antibody
418 (Invitrogen) (MDCK cells) were used to detect GFP-tagged proteins. Anti-mCherry (mouse
419 monoclonal, Invitrogen) (HEK293T cells), Anti-mCherry (rabbit monoclonal, Invitrogen) (MDCK
420 cells), Alexa Fluor 568-conjugated Goat anti-mouse antibody (Invitrogen) (HEK293T cells), and
421 Alexa Fluor 568-conjugated Goat anti-rabbit (Invitrogen) (MDCK cells) were used to detect
422 mCherry. Biotinylated proteins were identified with Alexa Fluor 647-conjugated streptavidin
423 (Invitrogen). Primary antibodies were incubated for 1 hr (1:1000 dilution in PBS with 1% BSA and
424 0.3% Triton X-100) and secondary antibodies were incubated for 30 min (1:1000 dilution in PBS
425 with 1% BSA and 0.3% Triton X-100). Cells were imaged using a Leica Microsystems Stellaris 5
426 confocal setup with 63x/1.40 NA oil objective. Images were reconstructed using ImageJ.

427

428 **Image analysis:** All analysis was done in ImageJ. In order to reduce background and
429 oversaturated pixel contribution, all images were processed with a Gaussian filter with a sigma of
430 11 (HEK images) or 15 (MDCK images). The filtered image was then subtracted from the original
431 image. CibN/ECibN expression was used to determine the area to be measured, and a threshold
432 mask was created using the CIB-GFP signal using a threshold minimum of 50 on the Threshold
433 tool. Membrane ROI's were hand-chosen with the wand tool from the CibN/ECibN GFP channel
434 using this mask. Since CibN and ECibN localize to the cell membrane, the ROIs only contain the
435 plasma membrane. Higher Gaussian sigmas were used on MDCK cells due to the lower
436 expression of ECibN. The ROIs were used for both fluorescence intensity measurements and
437 colocalization analysis. Colocalization analysis was carried out on the processed images using

438 the Coloc2 plugin with Costes threshold regression, a PSF of 3, and 10 Costes randomizations.
439 Unthresholded Pearson's coefficients were used from the outputs. Intensity measurements for all
440 channels were taken on the processed images using the Multi Measure functionality on the ROI
441 manager.

442

443 **Sample preparation for MS and Western Blot analysis:** MDCK cells stably expressing
444 Ecad-LAB or Ecad-Turbo and HEK cells transiently transfected with LAB were cultured on p150
445 dishes. The cells were incubated with 100 μM biotin and exposed to blue light on a 10 min on/off
446 cycle for 1 hr (LAB, Ecad-LAB) or exposed to 100 μM biotin alone (Ecad-Turbo). Control cells
447 were kept in darkness (LAB, Ecad-LAB) or without exogenous biotin (Ecad-Turbo). After
448 incubation, cells were washed three times with PBS, scraped, and centrifuged. Pelleted MDCK
449 cells were resuspended in M2 lysis buffer (50 mM Tris pH 7.5, 150 mM NaCl, 1% sodium dodecyl
450 sulfate (SDS), 1% Triton X-100 (Muinao et al., 2018)) with 5 μL/mL of protease inhibitor mixture
451 (Sigma-Aldrich), and 1 μL/mL Benzonase Nuclease (250 U/μL) (Millipore-Sigma). Pelleted
452 HEK293T cells were resuspended in lysis buffer (50 mM Tris pH 7.5, 150 mM NaCl, 0.4% sodium
453 dodecyl sulfate (SDS), 1% octyl phenoxy poly(ethyleneoxy) ethanol (IGEPAL CA-630), 1.5 mM
454 $MgCl_2$, 1 mM EGTA) with 2 μL/mL of protease inhibitor mixture (Sigma-Aldrich), and 1 μL/mL
455 Benzonase Nuclease (250 U/μL) (Millipore-Sigma). The lysate was flash frozen in dry ice and
456 quickly thawed at 37 °C. The lysate was then incubated for 30 min at 4 °C and sonicated at 30%
457 duty ratio for 1 min. Next, the lysate was centrifuged at 13,000 rpm for 30 min at 4 °C. After that,
458 the concentrations of the supernatant were measured with an RC DC protein assay kit (Bio-Rad).
459 Supernatant concentration was adjusted to the lowest concentration and lysis buffer was added
460 to bring all volumes to 1mL. Supernatant was incubated with 50 μL (HEK293T) or 100 μL (MDCK)
461 of superparamagnetic streptavidin conjugated beads (Dynabeads MyOne Streptavidin C1,

462 Invitrogen) and rotated overnight at 4 °C. The next day, beads were washed with the lysis buffer.
463 Then, beads were washed with the 2% SDS in 50 mM Tris, pH 7.4, and twice with lysis buffer.

464 For MS sample preparation, magnetic beads loaded with biotinylated proteins were
465 washed three times with 50 mM ammonium bicarbonate (NH_4HCO_3) and resuspended in 60 µL
466 of 50 mM NH_4HCO_3 containing 5 µg of trypsin for overnight digestion at 37 °C in a shaker. The
467 resulting peptides were recovered from the beads by removing the supernatant after pelleting the
468 beads via magnetic holder, and tryptic peptides from the supernatant were dried in a vacuum
469 centrifuge and reconstituted in 0.1% formic acid. Tryptic peptides were analyzed using nano-scale
470 liquid chromatographic tandem mass spectrometry (nLC-MS/MS).

471 For MDCK western blots, whole cell lysate was used, with an identical amount of total
472 protein loaded in each lane, determined using DC assay concentration measurements. Lysate
473 was run on a 4-15% Mini-Protean TGX Precast Protein Gel (Bio-Rad) before being transferred to
474 a nitrocellulose membrane and stained for biotin using HRP-conjugated Anti-biotin (1:1000
475 dilution, Cell Signaling Technology). WesternBright ECL HRP substrate (Advansta) was used to
476 detect the protein.

477 For the HEK293T western blots, after capturing the biotinylated proteins, beads were
478 incubated with 60 µl of 2.5 mM biotin at 95 °C for 5 min. Then, the eluted biotinylated proteins
479 were collected and run on a 4-15% Mini-Protean TGX Precast Protein Gel (Bio-Rad) before being
480 transferred to a nitrocellulose membrane and stained for biotin, GFP, and mCherry using Sta
481 conjugated with Horseradish Peroxidase (HRP) (1:1000 dilution, Invitrogen), Anti-GFP antibody
482 (rabbit polyclonal, 1:1000 dilution, Rockland Immunochemicals) and Alexa Fluor 488-conjugated
483 Goat anti-rabbit antibody (1:1000 dilution, Life Technologies), and Anti-mCherry (mouse
484 monoclonal, 1:1000 dilution Invitrogen) and HRP-conjugated Goat anti-mouse antibody (1:1000

485 dilution, Invitrogen). WesternBright ECL HRP substrate (Advansta) was used to detect the protein.
486 Images were acquired using Image Lab software from Bio-Rad.

487

488 **Mass Spectrometry:** For each sample, an equal volume of peptide was loaded onto a
489 disposable Evotip C18 trap column (Evosep Biosystems, Denmark) as per the manufacturer's
490 instructions. Briefly, Evotips were wetted with 2-propanol, equilibrated with 0.1% formic acid, and
491 then loaded using centrifugal force at 1200 g. Evotips were subsequently washed with 0.1%
492 formic acid, and then 200 µL of 0.1% formic acid was added to each tip to prevent drying. The
493 tipped samples were subjected to nanoLC on an Evosep One instrument (Evosep Biosystems).
494 Tips were eluted directly onto a PepSep analytical column, dimensions: 8cm x 150µm, C18
495 column with 1.5 µm particle size (PepSep, Denmark), and a ZDV spray emitter (Bruker
496 Daltronics). Mobile phases A and B were water with 0.1% formic acid (v/v) and 80/20/0.1%
497 ACN/water/formic acid (v/v/v), respectively. The standard pre-set method of 60 samples-per-day
498 was used, which is a 26 min gradient.

499 Mass spectrometry was performed on a hybrid trapped ion mobility spectrometry-
500 quadrupole time of flight mass spectrometer (timsTOF Pro, Bruker Daltonics) with a modified
501 nano-electrospray ion source (CaptiveSpray, Bruker Daltonics), as described previously (Shafraz
502 et al., 2020). Mass spectrometry raw files were processed with MsFragger (Yu et al., 2020) as
503 previously described (Shafraz et al., 2020). Volcano and PCA plots were generated using
504 Spectronaut viewer. Known contamination proteins (Hodge et al., 2013) were removed, with
505 further contamination filtering done by removing all non-canine proteins, with the exception of
506 Cry/CIB from Arabidopsis (Ecad-LAB samples) and GFP from Aequorea (both), and filtering out
507 all proteins categorized as "universal contaminants" by the software. A global background signal

508 was added using the background signal imputation method, where the software chooses the best
509 background signal to report as the precursor quantity. This allowed protein concentrations to be
510 compared between the light positive and light negative conditions and ameliorated issues where
511 proteins at too low concentrations in the negative condition could not be compared to the light
512 positive condition. Only proteins that had two or more unique peptides detected were included in
513 analysis. A Q-value of 0.05 was used to determine candidate threshold. Ecad-LAB runs and Ecad-
514 Turbo runs were analyzed in separate files.

515

516 **Data Availability:** MS raw spectra data can be found in the MassIVE database at:

517 http://massive.ucsd.edu/ProteoSAFe/status.jsp?task=7dbf769e09fe410ba03980935ab8f048

518

519 **Acknowledgements:** This research was supported in part by the National Institute of General
520 Medical Sciences of the National Institutes of Health (R01GM121885) and the National Science
521 Foundation (MCB-2022385). We thank Dr. Gabriela Grigorean for performing LC-MS/MS and
522 data analysis in Proteomics Core Facility of the Genome Center at University of California, Davis.

523

524 **Author contributions:** O.S., C.M.O.D., and S.S. designed research; O.S. and C.M.O.D.
525 collected and analyzed data; O.S., C.M.O.D., and S.S. wrote the paper.

526

527

528 **Figure Legends**

529 **Figure 1: Light Activated BioID (LAB) dimerizes upon blue light illumination.** (a)
530 Schematic of LAB construct used in HEK293T cells. Fragment of Split-TurboID (N) and
531 *Arabidopsis* protein CIB1 were fused onto prenylated plasma membrane targeted Enhanced
532 Green Fluorescent Protein (pmEGFP) that localizes to the plasma membrane (CibN). The
533 complementary Split-TurboID (C) fragment was fused to blue-light receptor protein Cryptochrome
534 2 (CRY2) and mCherry fluorescent protein (CryC) and expressed in the cytoplasm. When
535 exposed to blue light, CRY2 interacts with CIB1 and reconstitutes the split-TurboID, which
536 generates reactive biotin for proximity labeling. Both constructs were transiently co-expressed in
537 HEK293T cells. (b) Confocal images show CibN localizing to the membrane and CryC diffused in
538 the cytoplasm of the cells. When excited with a 488 nm laser, CryC localized to the membrane in
539 seconds and dissociated completely in about 600 sec. Scale bar 3 μm. (c) A region of the
540 membrane was excited with 488 nm laser and CryC accumulation was monitored. CryC
541 accumulated at the membrane region in sub-seconds. Scale bar 3 μm. (d) CryC and CibN
542 intensity was measured across the yellow line in *(c)* with vertical black dashed lines delineating
543 the membrane on the graph. The fluorescence intensity measurements showed a strong
544 correlation between CryC and CibN after light exposure. (e) Integrated CryC (red) and CibN
545 (green) intensity was measured in the yellow box in *(c)* over time, with the vertical black dashed
546 line indicating 488 nm laser excitation. CryC fluorescence reached the maximum intensity within
547 seconds, while CibN fluorescence remained constant.

548

549 **Figure 2: LAB biotinylation is light-dependent.** CibN and CryC were transiently co-
550 expressed in HEK 293T cells and, in the presence of 100 μM biotin, were exposed to 10 min

551 cycles of alternating blue light and darkness for 1hr. The cells were fixed and stained for EGFP,
552 mCherry, and biotin. (a) Schematic of light exposure sequence used. (b) Immunofluorescence
553 showed that in the presence (+) of exogenous biotin and light, membrane-localized CibN (EGFP)
554 and CryC (mCherry) dimerized and biotinylated proteins (Streptavidin, Sta) in the vicinity of the
555 plasma membrane, with composite images confirming the colocalization of CibN, CryC, and Sta.
556 (c) In the absence (-) of blue light, (d) in the absence of added biotin or (e) in the absence of both
557 biotin and light, no biotinylation was observed. When only (f) CryC or (g) CibN were expressed,
558 no biotinylation was detected, showing CibN and CryC dimerization are essential for proximity
559 labeling. To facilitate an unbiased visual comparison of fluorescence intensities in (*b* - *g*), the
560 panels in each column display identical minimum and maximum intensities. (h) Bar graph of CryC,
561 CibN, and Sta fluorescent intensity averaged across number of cells from three biological
562 replicates show significant biotinylation occurring only in the presence of light and biotin. CryC
563 intensity proximal to membrane is significant only in the light positive conditions, showing it
564 localizes with the membrane only in the presence of light. Fluorescent intensity of CryC and Sta
565 proximal to membrane region was normalized to CibN to account for variation in CibN expression
566 levels in different cells. Normalized fluorescence intensities are tabulated in table S1 while
567 corresponding p-values are tabulated in table S3. (i) Average Pearson's coefficient shows CibN
568 and CryC colocalize in the presence of light, while Sta colocalizes to CibN only in the presence
569 of light and biotin. Average Pearson's coefficient values are tabulated in table S2 while
570 corresponding p-values are tabulated in table S4. All scale bars 10 μm. Errors: s.e. n= number of
571 cells from three biological replicates for all conditions.

572

573 **Figure 3: Ecad-CibN and CryC dimerize and biotinylate only when exposed to light.**
574 (a) Schematic of Ecad-LAB. Split-TurboID (N), and CIB1 were fused onto the C terminus of Ecad-

575 EGFP to create ECibN. CryC was expressed in the cytoplasm. Both constructs were stably co-
576 expressed in MDCK cells. When exposed to blue light, dimerization of ECibN and CryC
577 reconstitutes the split-TurboID, which generates reactive biotin for proximity labeling. (b) Cells
578 incubated with 100 μM biotin were illuminated with blue light, for an hour, on a 10 min on/off cycle.
579 The cells were fixed and stained for EGFP, mCherry and biotin. ECibN localizes to the intercellular
580 junction, and in the presence (+) of light and biotin dimerizes with CryC resulting in the
581 biotinylation of proteins close to the membrane, which is confirmed with composite images
582 showing the colocalization of CibN, CryC, and Sta. (c) In the absence (-) of light, (d) biotin or (e)
583 both, no biotinylation is observed. When only (f) CryC or (g) ECibN were transiently expressed in
584 MDCK cells, no biotinylation was observed. To facilitate an unbiased visual comparison of
585 fluorescence intensities in (*b* - *g*), the panels in each column display identical minimum and
586 maximum intensity. (h) Fluorescent intensity of CryC, ECibN, and Sta, normalized to ECibN
587 intensity to account for variation in expression levels in different cells, shows that CryC only
588 associates to the membrane in light and biotinylation is detected only in the presence of light and
589 biotin. Normalized fluorescence intensities are tabulated in table S5 while corresponding p-values
590 are tabulated in table S7. (i) Average Pearson's coefficient shows ECibN and CryC colocalize in
591 the presence of light, while Sta colocalizes to ECibN only in the presence of light and biotin.
592 Average Pearson's coefficient values are tabulated in table S6 while corresponding p-values are
593 tabulated in table S8. All scale bars are 20 μm. Errors: s.e. n = 156 cells evenly split between
594 three biological replicates for all conditions.

595

596 **Figure 4: Mass spectrometry shows that Ecad-LAB is more accurate and precise**
597 **than Ecad-Turbo.** a) Volcano plot showing the enrichment of biotinylated proteins in Ecad-LAB,
598 in the presence (positive; white) and absence (negative; pink) of light. Known Ecad-associated

599 proteins are labeled in different colors and are highly enriched. b) Volcano plot showing the
600 enrichment of biotinylated proteins in Ecad-Turbo, in the presence (positive; white) and absence
601 (negative; pink) of biotin. There are many more negative “hits” in Ecad-Turbo compared to Ecad-
602 LAB. c) Every hit (positive candidates, negative candidates, and non-candidates) in Ecad-LAB
603 was also a hit in Ecad-Turbo, with the expected exceptions of Cry and CIB. d) Comparison of
604 positive/negative signals for several key Ecad binding proteins highlighted in (*a*). Ecad-LAB has
605 a universally higher signal ratio. Proteins without any signal in the negative condition were given
606 an arbitrarily high ratio value (*) to avoid dividing by zero. e) Signal ratio for broad categories of
607 proteins, graphed on a log scale. Categories were chosen based on previously published
608 categories in the Ecad interactome (Shafraz et al., 2020), as follows: A: Adhesion Receptors; B:
609 Cytoskeletal components and motors; C: Kinases and Phosphatases; D: Membrane binding
610 adaptors, receptors, and transporters; E: Other/Unknown/Secreted; F: Actin and microtubule
611 binding and dynamics-associated; G: Adaptors; H: Metabolic Enzymes; I: Chaperone, trafficking,
612 degradation, and GTPase regulation; J: DNA and Translation.

613

614

615

616 **References:**

617 Branon, T.C., Bosch, J.A., Sanchez, A.D., Udeshi, N.D., Svinkina, T., Carr, S.A., Feldman, J.L.,
618 Perrimon, N., and Ting, A.Y. (2018). Efficient proximity labeling in living cells and organisms with
619 TurboID. Nat Biotechnol *36*, 880-887.

620 Bugaj, L.J., Choksi, A.T., Mesuda, C.K., Kane, R.S., and Schaffer, D.V. (2013). Optogenetic
621 protein clustering and signaling activation in mammalian cells. Nature Methods *10*, 249-252.

622 Chen, R., Zhang, N., Zhou, Y., and Jing, J. (2022). Optical Sensors and Actuators for Probing
623 Proximity-Dependent Biotinylation in Living Cells. Frontiers in Cellular Neuroscience *16*.

624 Cho, K.F., Branon, T.C., Rajeev, S., Svinkina, T., Udeshi, N.D., Thoudam, T., Kwak, C., Rhee, H.-
625 W., Lee, I.-K., Carr, S.A.*, et al.* (2020a). Split-TurboID enables contact-dependent proximity
626 labeling in cells. Proceedings of the National Academy of Sciences *117*, 12143-12154.

627 Cho, K.F., Branon, T.C., Udeshi, N.D., Myers, S.A., Carr, S.A., and Ting, A.Y. (2020b). Proximity
628 labeling in mammalian cells with TurboID and split-TurboID. Nature Protocols *15*, 3971-3999.

629 Choi-Rhee, E., Schulman, H., and Cronan, J.E. (2004). Promiscuous protein biotinylation by
630 Escherichia coli biotin protein ligase. Protein Science *13*, 3043-3050.

631 Geri, J.B., Oakley, J.V., Reyes-Robles, T., Wang, T., McCarver, S.J., White, C.H., Rodriguez-
632 Rivera, F.P., Parker, D.L., Jr., Hett, E.C., Fadeyi, O.O.*, et al.* (2020). Microenvironment mapping
633 via Dexter energy transfer on immune cells. Science *367*, 1091-1097.

634 Guo, Z., Neilson, L.J., Zhong, H., Murray, P.S., Zanivan, S., and Zaidel-Bar, R. (2014). E-cadherin
635 interactome complexity and robustness resolved by quantitative proteomics. Science Signaling *7*,
636 rs7.

637 Hodge, K., Have, S.T., Hutton, L., and Lamond, A.I. (2013). Cleaning up the masses: exclusion
638 lists to reduce contamination with HPLC-MS/MS. Journal of Proteomics *88*, 92-103.

639 Kennedy, M.J., Hughes, R.M., Peteya, L.A., Schwartz, J.W., Ehlers, M.D., and Tucker, C.L.
640 (2010). Rapid blue-light-mediated induction of protein interactions in living cells. Nature Methods
641 *7*, 973-975.

642 Kim, D.I., Birendra, K.C., Zhu, W., Motamedchaboki, K., Doye, V., and Roux, K.J. (2014). Probing
643 nuclear pore complex architecture with proximity-dependent biotinylation. Proceedings of the
644 National Academy of Sciences of the United States of America *111*, E2453-2461.

645 Kim, D.I., Jensen, S.C., Noble, K.A., Kc, B., Roux, K.H., Motamedchaboki, K., and Roux, K.J.
646 (2016). An improved smaller biotin ligase for BioID proximity labeling. Molecular Biology of the
647 Cell *27*, 1188-1196.

648 Klewer, L., and Wu, Y.-W. (2019). Light-Induced Dimerization Approaches to Control Cellular
649 Processes. Chemistry – A European Journal *25*, 12452-12463.

650 Kotani, N., Gu, J., Isaji, T., Udaka, K., Taniguchi, N., and Honke, K. (2008). Biochemical
651 visualization of cell surface molecular clustering in living cells. Proceedings of the National
652 Academy of Sciences *105*, 7405-7409.

653 Liu, H., Yu, X., Li, K., Klejnot, J., Yang, H., Lisiero, D., and Lin, C. (2008). Photoexcited CRY2
654 Interacts with CIB1 to Regulate Transcription and Floral Initiation in Arabidopsis. Science *322*,
655 1535-1539.

656 Liu, Q., Zheng, J., Sun, W., Huo, Y., Zhang, L., Hao, P., Wang, H., and Zhuang, M. (2018). A
657 proximity-tagging system to identify membrane protein-protein interactions. Nature Methods *15*,
658 715-722.

659 Mair, A., Xu, S.-L., Branon, T.C., Ting, A.Y., and Bergmann, D.C. (2019). Proximity labeling of
660 protein complexes and cell-type-specific organellar proteomes in Arabidopsis enabled by
661 TurboID. eLife *8*, e47864.

662 Martell, J.D., Deerinck, T.J., Sancak, Y., Poulos, T.L., Mootha, V.K., Sosinsky, G.E., Ellisman,
663 M.H., and Ting, A.Y. (2012). Engineered ascorbate peroxidase as a genetically encoded reporter
664 for electron microscopy. Nature Biotechnology *30*, 1143-1148.

665 Muinao, T., Pal, M., and Boruah, H.P.D. (2018). Cytosolic and Transmembrane Protein Extraction
666 Methods of Breast and Ovarian Cancer Cells: A Comparative Study. J Biomol Tech *29*, 71-78.

667 Müller, M., Gräbnitz, F., Barandun, N., Shen, Y., Wendt, F., Steiner, S.N., Severin, Y., Vetterli, S.U.,
668 Mondal, M., Prudent, J.R.*, et al.* (2021). Light-mediated discovery of surfaceome nanoscale
669 organization and intercellular receptor interaction networks. Nature Communications *12*, 7036.

670 Qin, W., Cho, K.F., Cavanagh, P.E., and Ting, A.Y. (2021). Deciphering molecular interactions by
671 proximity labeling. Nature Methods *18*, 133-143.

672 Ramanathan, M., Majzoub, K., Rao, D.S., Neela, P.H., Zarnegar, B.J., Mondal, S., Roth, J.G., Gai,
673 H., Kovalski, J.R., Siprashvili, Z.*, et al.* (2018). RNA–protein interaction detection in living cells.
674 Nature Methods *15*, 207-212.

675 Roux, K.J., Kim, D.I., Raida, M., and Burke, B. (2012). A promiscuous biotin ligase fusion protein
676 identifies proximal and interacting proteins in mammalian cells. The Journal of Cell Biology *196*,
677 801-810.

678 Seath, C.P., Trowbridge, A.D., Muir, T.W., and MacMillan, D.W.C. (2021). Reactive intermediates
679 for interactome mapping. Chemical Society Reviews *50*, 2911-2926.

680 Shafraz, O., Xie, B., Yamada, S., and Sivasankar, S. (2020). Mapping transmembrane binding
681 partners for E-cadherin ectodomains. Proceedings of the National Academy of Sciences *117*,
682 31157-31165.

683 Taslimi, A., Zoltowski, B., Miranda, J.G., Pathak, G.P., Hughes, R.M., and Tucker, C.L. (2016).
684 Optimized second-generation CRY2-CIB dimerizers and photoactivatable Cre recombinase.
685 Nature Chemical Biology *12*, 425-430.

686 Wang, Q., and Lin, C. (2020). A structural view of plant CRY2 photoactivation and inactivation.
687 Nature Structural & Molecular Biology *27*, 401-403.

688 Wang, Y., Gao, H., Na, X.-L., Dong, S.-Y., Dong, H.-W., Yu, J., Jia, L., and Wu, Y.-H. (2016). Aniline
689 Induces Oxidative Stress and Apoptosis of Primary Cultured Hepatocytes. In International Journal
690 of Environmental Research and Public Health.

691 Xie, B., Maker, A., Priest, A.V., Dranow, D.M., Phan, J.N., Edwards, T.E., Staker, B.L., Myler, P.J.,
692 Gumbiner, B.M., and Sivasankar, S. (2022). Molecular mechanism for strengthening E-cadherin

693 adhesion using a monoclonal antibody. Proceedings of the National Academy of Sciences *119*,
694 e2204473119.

695 Yu, F., Haynes, S., Teo, G.C., Avtonomov, D., Polasky, D., and Nesvizhskii, A. (2020). Fast
696 quantitative analysis of timsTOF PASEF data with MSFragger and IonQuant (bioRxiv).

697 Zhai, Y., Huang, X., Zhang, K., Huang, Y., Jiang, Y., Cui, J., Zhang, Z., Chiu, C.K.C., Zhong, W.,
698 and Li, G. (2022). Spatiotemporal-resolved protein networks profiling with photoactivation
699 dependent proximity labeling. Nature Communications *13*, 4906.

700

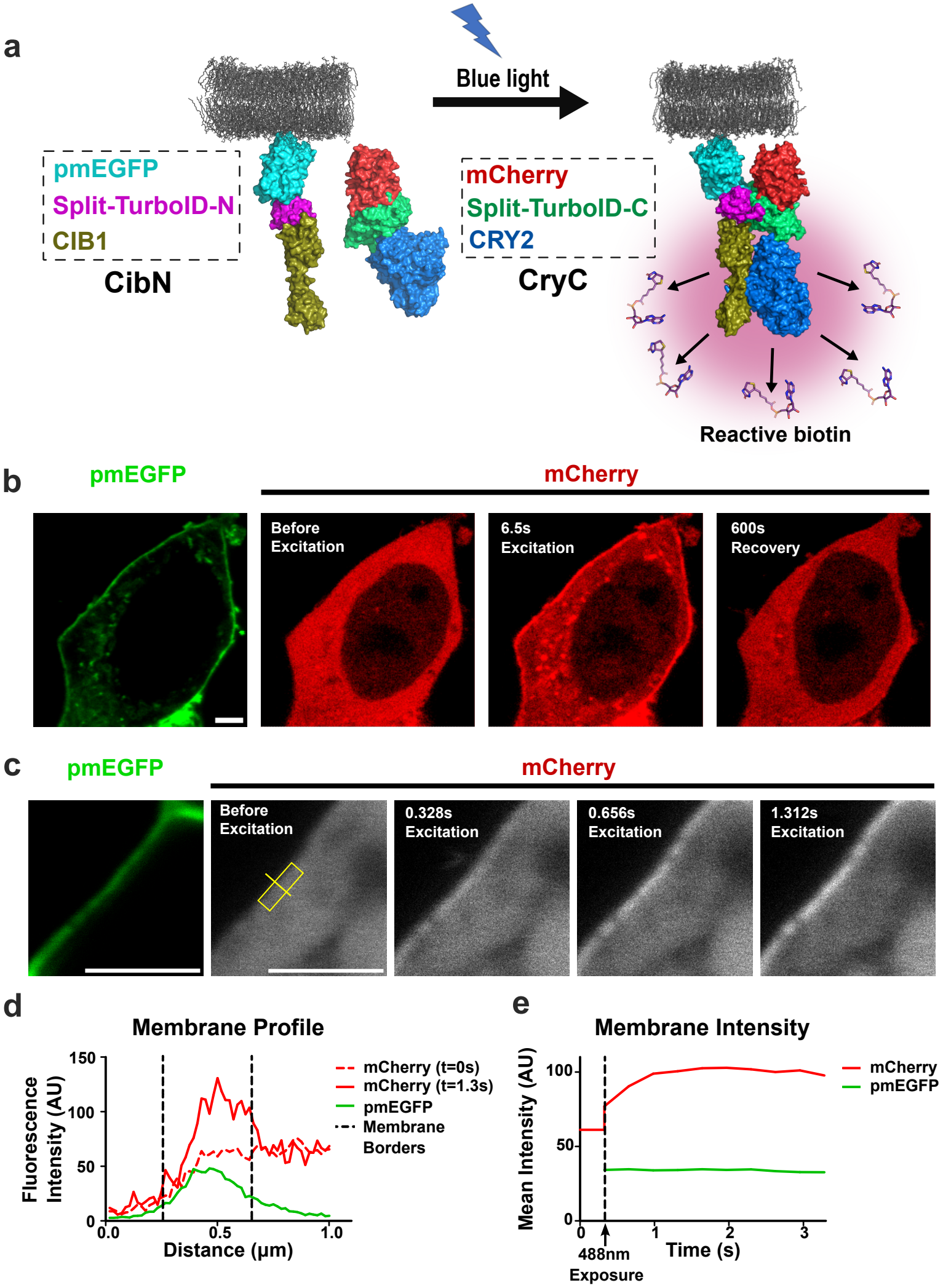
a
Blue light
pmEGFP
Split-TurboID-N
CIB1
CibN
mCherry
Split-TurboID-C
CRY2
CryC
Reactive biotin
b
pmEGFP
mCherry
Before Excitation
6.5s Excitation
600s Recovery
c
pmEGFP
mCherry
Before Excitation
0.328s Excitation
0.656s Excitation
1.312s Excitation
d
Membrane Profile
Fluorescence Intensity (AU)
150
100
50
0
0.0
0.5
1.0
Distance (μm)
mCherry (t=0s)
mCherry (t=1.3s)
pmEGFP
Membrane Borders
e
Membrane Intensity
Mean Intensity (AU)
100
50
0
0
1
2
3
Time (s)
488nm Exposure
mCherry
pmEGFP

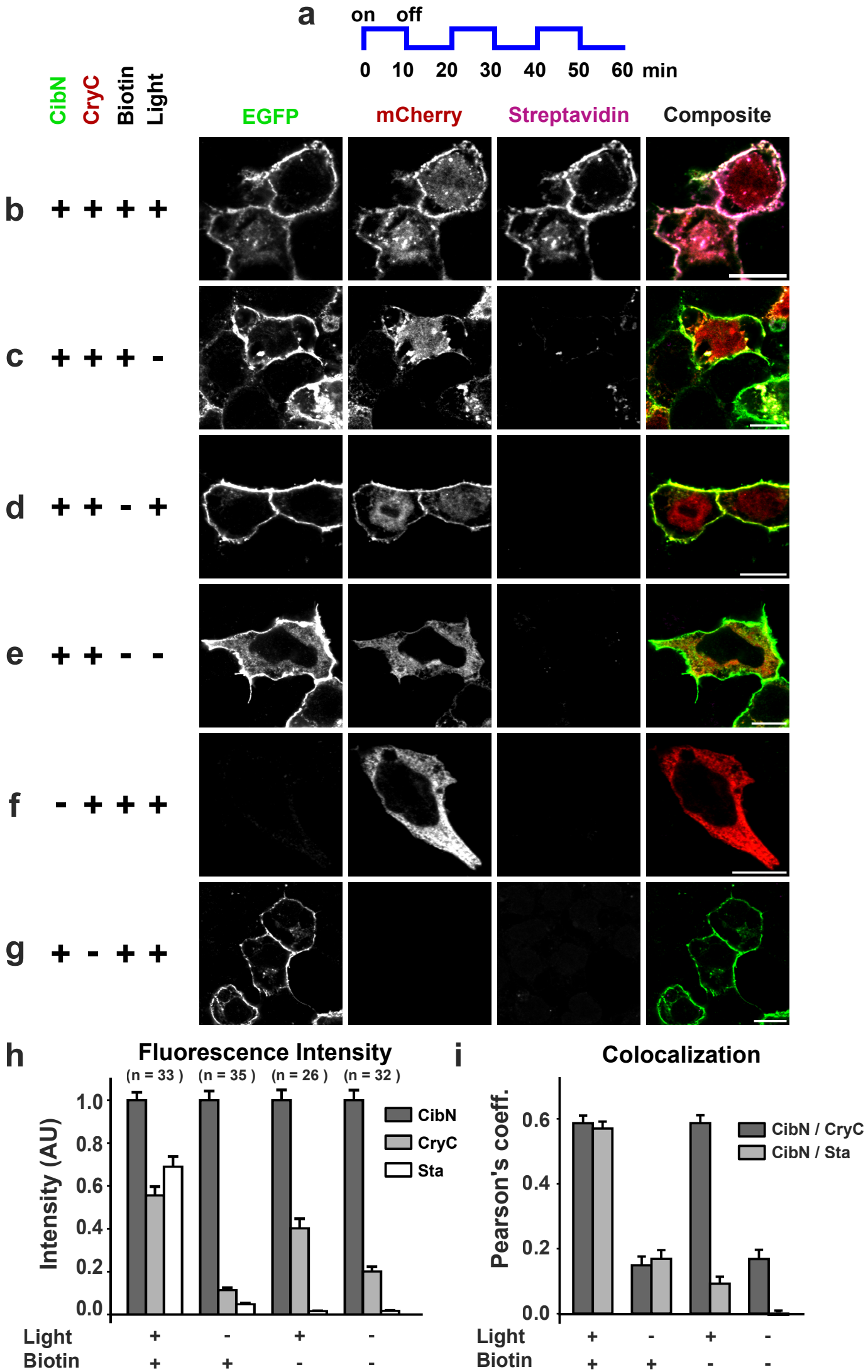
a
on
off
0
10
20
30
40
50
60
min
CibN
CryC
Biotin
Light
EGFP
mCherry
Streptavidin
Composite
b + + + +
c + + + -
d + + - +
e + + - -
f - + + +
g + - + +
h
Fluorescence Intensity
(n = 33)
(n = 35)
(n = 26)
(n = 32)
Intensity (AU)
1.0
0.8
0.6
0.4
0.2
0.0
CibN
CryC
Sta
Light + - + -
Biotin + + - -
i
Colocalization
Pearson's coeff.
0.6
0.4
0.2
0.0
CibN / CryC
CibN / Sta
Light + - + -
Biotin + + - -

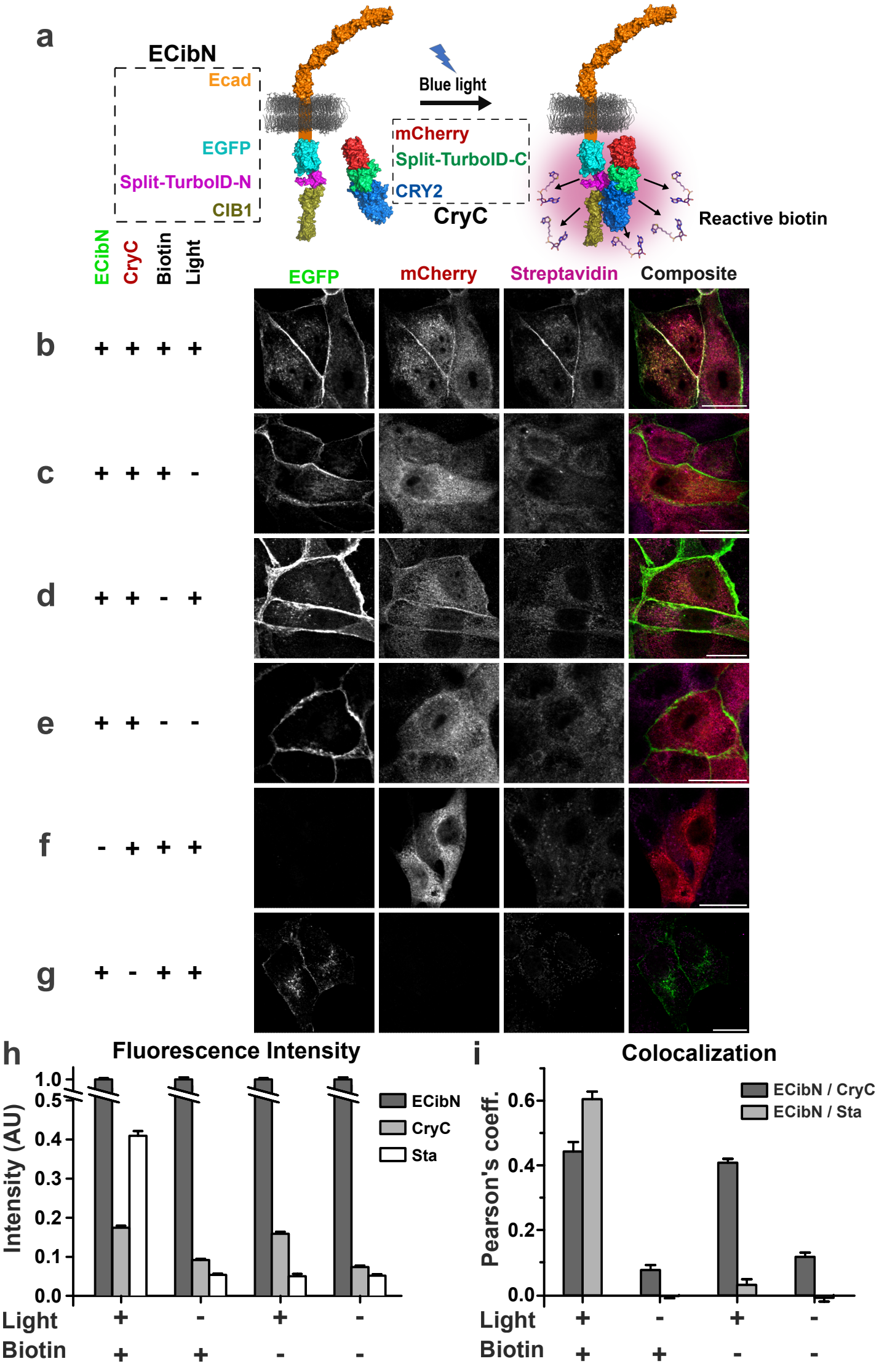
a
ECibN
Ecad
EGFP
Split-TurboID-N
CIB1
Blue light
mCherry
Split-TurboID-C
CRY2
CryC
Reactive biotin
ECibN
CryC
Biotin
Light
EGFP
mCherry
Streptavidin
Composite
b + + + +
c + + + -
d + + - +
e + + - -
f - + + +
g + - + +
h
Fluorescence Intensity
Intensity (AU)
1.0
0.5
0.4
0.3
0.2
0.1
0.0
ECibN
CryC
Sta
Light + - + -
Biotin + + - -
i
Colocalization
Pearson's coeff.
0.6
0.4
0.2
0.0
ECibN / CryC
ECibN / Sta
Light + - + -
Biotin + + - -

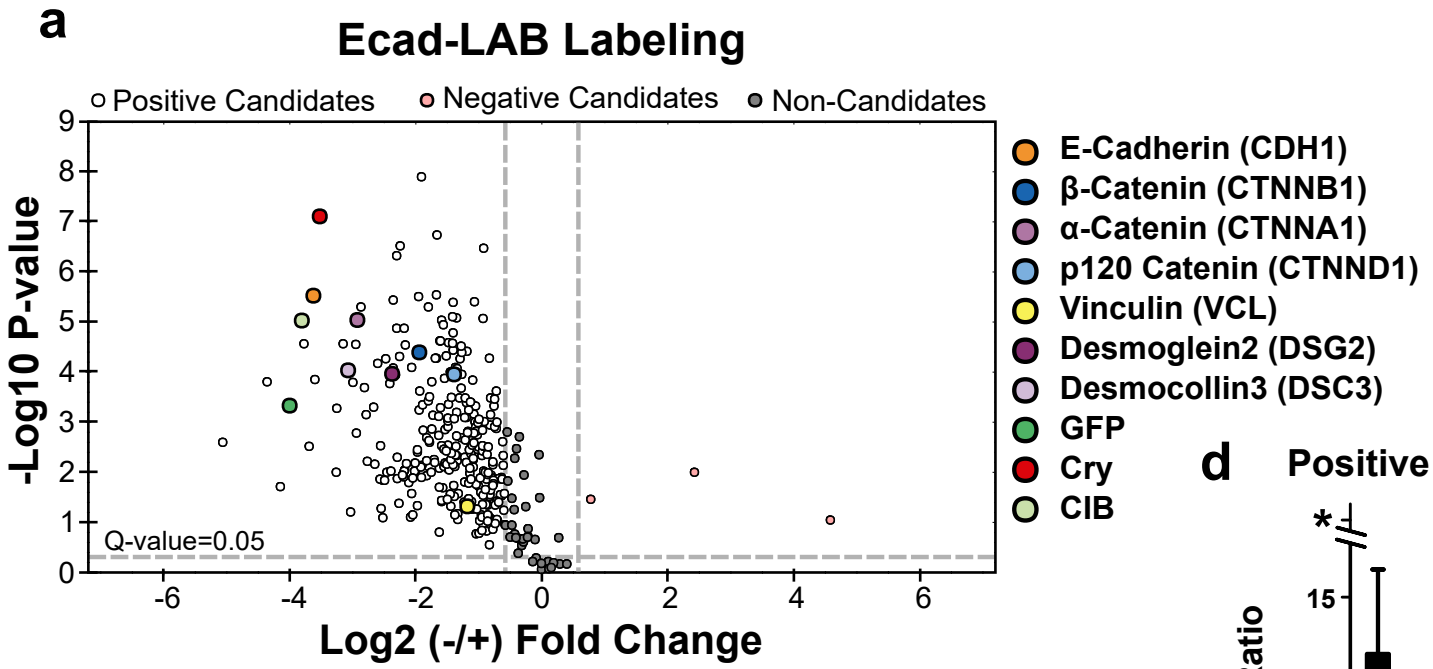
a
Ecad-LAB Labeling
Positive Candidates
Negative Candidates
Non-Candidates
-Log10 P-value
Log2 (-/+) Fold Change
Q-value=0.05
E-Cadherin (CDH1)
β-Catenin (CTNNB1)
α-Catenin (CTNNA1)
p120 Catenin (CTNND1)
Vinculin (VCL)
Desmoglein2 (DSG2)
Desmocollin3 (DSC3)
GFP
Cry
CIB

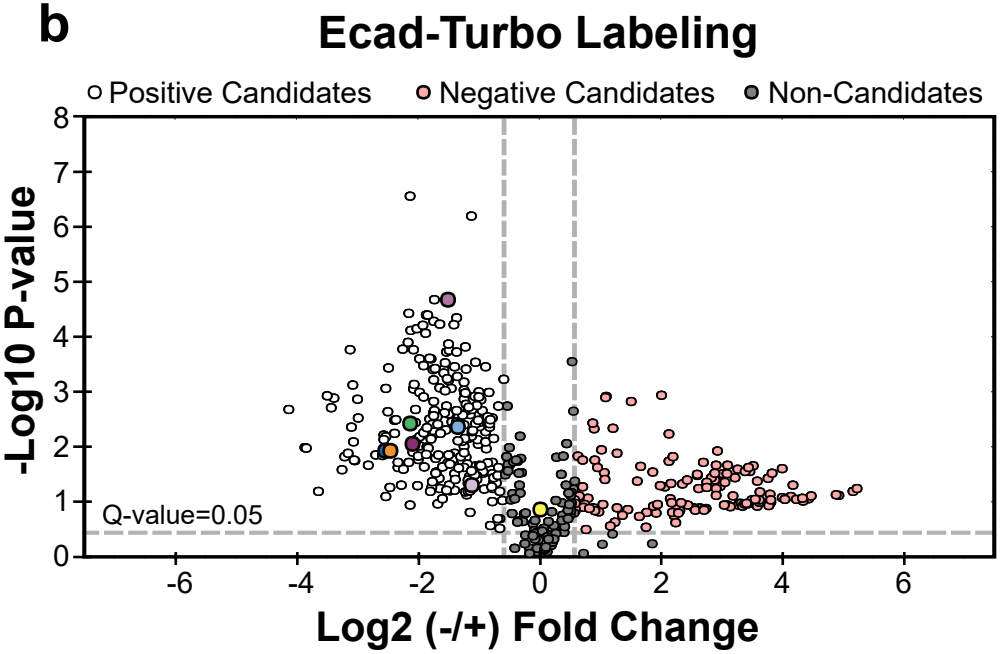
b
Ecad-Turbo Labeling
Positive Candidates
Negative Candidates
Non-Candidates
-Log10 P-value
Log2 (-/+) Fold Change
Q-value=0.05

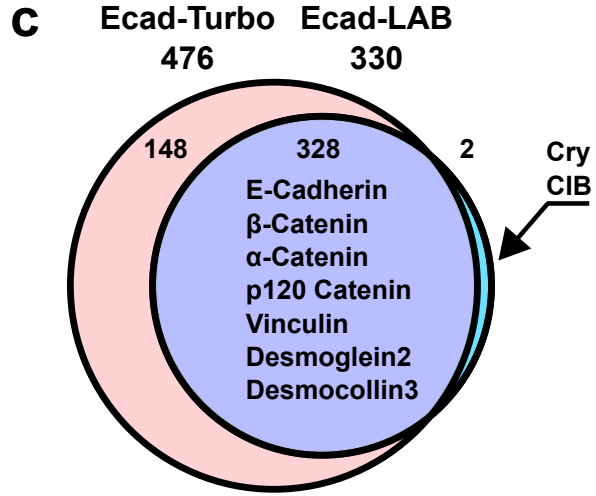
c
Ecad-Turbo
476
Ecad-LAB
330
148
328
2
Cry
CIB
E-Cadherin
β-Catenin
α-Catenin
p120 Catenin
Vinculin
Desmoglein2
Desmocollin3

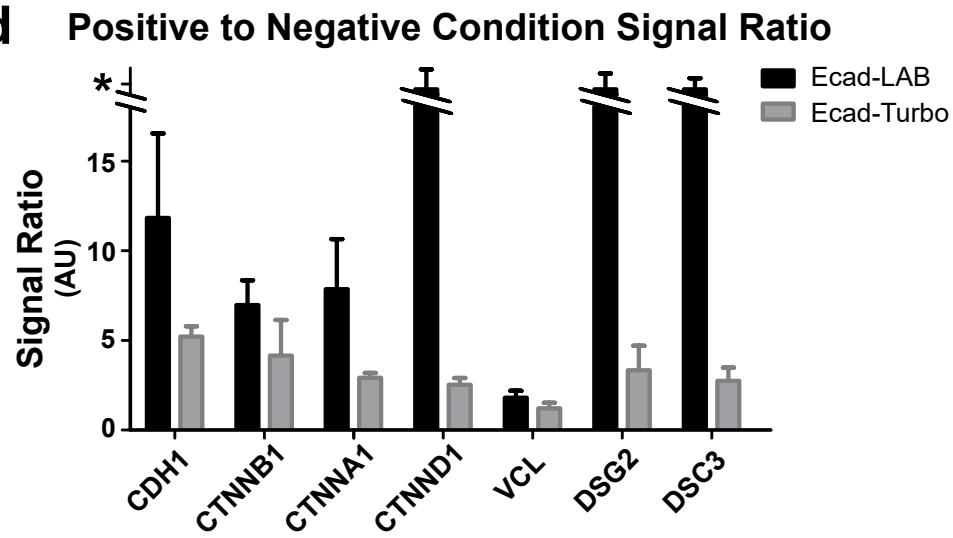
d
Positive to Negative Condition Signal Ratio
Ecad-LAB
Ecad-Turbo
Signal Ratio (AU)
CDH1
CTNNB1
CTNNA1
CTNND1
VCL
DSG2
DSC3

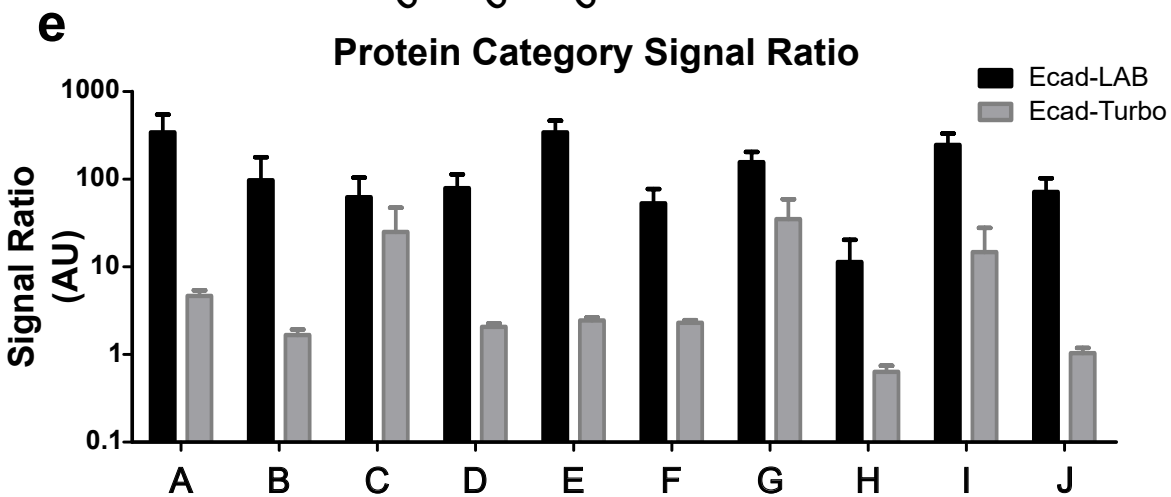
e
Protein Category Signal Ratio
Ecad-LAB
Ecad-Turbo
Signal Ratio (AU)
A
B
C
D
E
F
G
H
I
J